Solar-electric driven Heating and Cooling System with PCM-Storage for improved Grid Connection

Richard Schex[1], Andreas Krönauer[1], Michael Remy[1], Johannes Linn[1], Timo Korth[2], Felix Loistl[2], Christian Schweigler[2]

[1] Bavarian Center for Applied Energy Research (ZAE Bayern), Garching (Germany)

[2] Munich University of Applied Sciences, Munich (Germany)

Abstract

This study presents the coupling of a solar-electric driven air conditioning system (VRF, 3-pipe) with thermal storages based on Phase Change Material (PCM). The main objectives are the reduction of PV-related peak feed-in, to give a possibility for applying Demand Side Management and increasing self-consumption of such grid-connected PV-HVAC systems. To accomplish these goals the PCM-storage will be implemented directly in the refrigeration cycle of the system. Using PCM whose melting temperatures are adapted to the cooling process, cold/heat could be used directly without additional brine loops, accompanied by a negative effect on the EER. Furthermore the storage can be used to improve the system efficiency in case of discharge, which lowers the electrical demand when it is appropriate to reduce grid stress. Key issues are the development of the heat exchanger for the storage, the storage integration in the refrigeration cycle and the control strategies how to use the PCM-storage.

Keywords: Air Conditioning, Variable Refrigerant Flow (VRF), PCM, Heat Exchanger, Two-Phase-Flow, PV self-consumption, Demand Side Management

1. Introduction

Air Conditioning and heating based on electrically driven heat pumps is worldwide increasing in residential as well as in business buildings. Due to easy installation and easy access of the energy source/heat sink, air/air based systems are getting more and more relevant. The capability to store energy is limited in these systems. Systems with electric battery are expensive and sensible thermal storages do not fit well to the refrigeration cycle due to exergetic losses. The ability to store energy is mandatory to achieve better integration of PV-production for such combined systems. Especially in future when the numbers of installations will increase and capability to store energy is not given, a significant, negative impact on the electrical grid is expected, because the peak of cooling demand does not correspond to the peak of PV-production during the day.

The project approach is to integrate a thermal PCM-based storage into the refrigeration cycle of an air/air based 3-pipe VRF system. The efficiency of a heat pump corresponds directly to the temperature lift the compressor has to overcome. The approximately constant temperature of PCM at phase change can cause significant advantages in the system efficiency compared to sensible storage materials (Loistl et al., 2016). Therefore it is mandatory to choose materials whose melting temperature is appropriate for the desired effect of the heat storage, acting as heat sink, heat source or subcooler for the refrigeration cycle or as direct heat/cold storage.

doi:10.18086/swc.2017.28.16 Available at http://proceedings.ises.org

2. Modelling Phase

Several melting temperature ranges can be taken into account for implementing the PCM into the system. To get an idea which ranges will be most promising for the integration of PV-production and for the design of the entire system, load and PV-yield simulations have been made in TrnSys. The model consists of transient load simulations of a specific office building in which a pilot installation, based on a 3-pipe VRF system will be built up. Furthermore it contains transient PV-yield simulations, varying the installed peak-power. To simulate the theoretically possible thermal supply of the PV-driven heat pump the model is also fed with ambient temperature- and part load- dependent data of the EER/COP.

To gain reliable load data of the specific building, the known building characteristics and its geometry had been set up in the TRNBuild Editor. The building which is considered is located in Garching, in the south of Germany. It can be classified as a light construction building. The heating and cooling system supplies offices, laboratories and a small server room. The major part of the equipped building is shown in Figure 1.

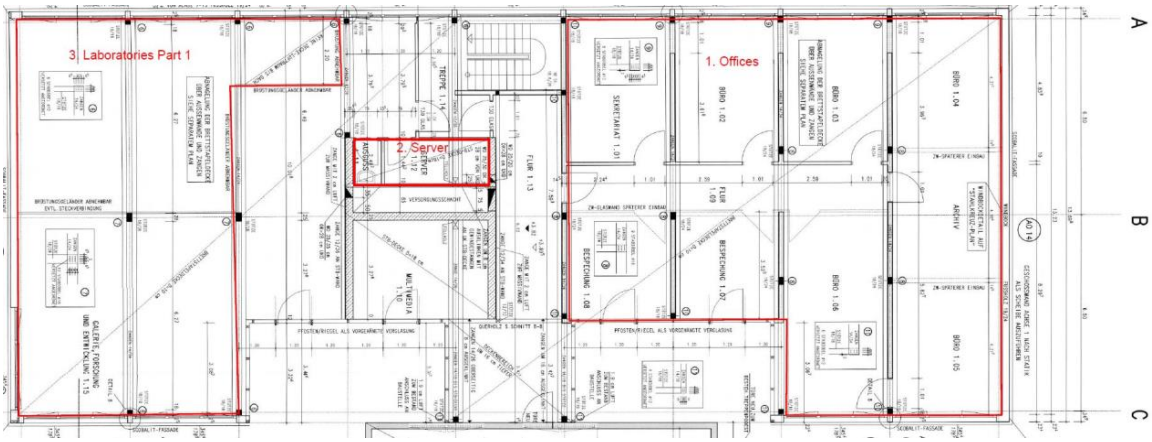

Figure 1 Main part of the institute building which will be equipped with Indoor Units (IU).

The main thermal features and data of the building are shown in table 1.

Tab. 1: General data and main thermal features of the modeled institute building in Garching.

Main thermal features of the building	
	U Value
Wooden structured external wall	0.24 W/m²K
External Roof	0.18 W/m²K
On-ground concrete floor slab	0.25 W/m²K
Insulated glazing	1.1 W/m²K
General data of building	
Location	Garching, N 48°15´, E 11° 40´
Floor surface Offices	160 m²
Floor surface Laboratories	150 m²
Air change rate	40 m³/h·person
Cooling/Heating set point temperatures	24 °C – 21 °C

For the PV-yield simulation the Standard TrnSys Type 194b for Photovoltaic-Arrays including inverter losses is used. For the investigation the reachable PV-yield was maximized using PV-panels facing south with an inclination of 30°. Under typical operating conditions, there is only limited congruence of PV-generator yield and electric building load. Thus, the storage is applied in order to accomplish a better match, avoiding losses of the possible PV-yield.

The pilot installation will be equipped with a Fujitsu V-II R VRF-System. To implement this system to the model the part-load and ambient temperature dependent data was fed in. This data is published by Fujitsu down to a part-load-ratio of 50%. (Fujitsu, 2014)

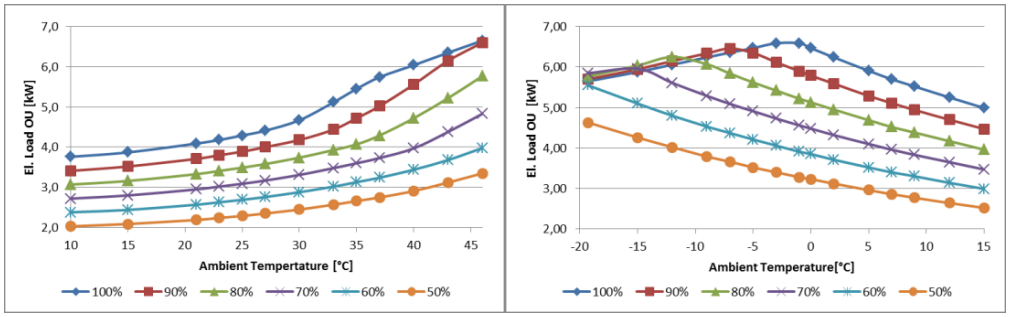

Figure 2 Electrical Load depending on ambient temperature and part-load ratio for cooling (left) and heating mode (right). Database for Fujitsu V-II R Type 72GALH with a rated cooling capacity of 22.4 kW and a rated heating capacity of 25 kW. The nominal electrical load is specified with 5.5 kW.

Figure 2 shows the electrical load of the Outdoor Unit 72GALH of the Fujitsu-System. Every curve represents a different part-load of the system in a range from 50% to 100%. Down to a part load ratio of 50% the EER as well as the COP depends mainly on the ambient temperature and only slightly on the part load of the system. A curve fitting method was used to get continuous data for the electrical load within the known ranges. Using the entire model it is possible to determine sizing and design parameters. Also an assessment of storage temperature levels can be made with the target of maximum reduction of grid stress caused by PV feed in.

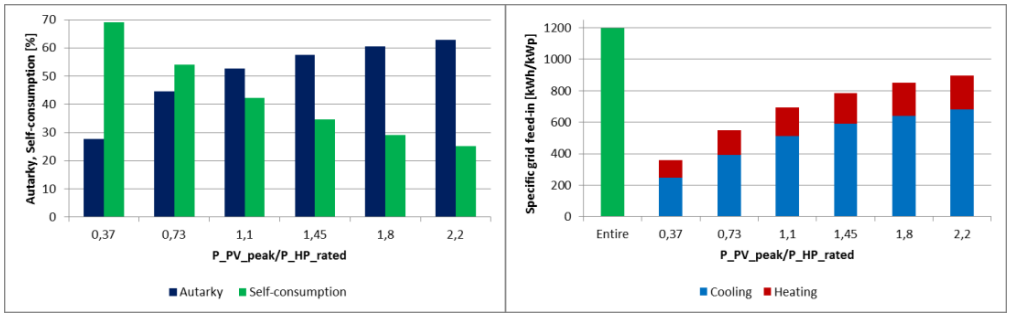

Figure 3 Autarky and self-consumption of system for different PV-installation (left). Specific remaining grid feed-in (right).

Figure 3 on the left hand side shows the possible autarky and self-consumption rate of the PV-HVAC system according to the electric power ratio of installed PV power related to the electric power rating of the heat pump. The right hand side shows the remaining grid feed-in during cooling and heating according to the above mentioned power ratio. Weniger et al. (2015) already shows that oversizing of the PV-generator in PV-storage systems leads to a saturation of autarky, while self-consumption is decreasing. Consequently, PV-peak feed in to the grid is increased. This effect can only be reduced by non-economic, oversized storages. The residual feed in to the electrical grid on the right figure is divided into the main cooling (blue) and main heating (red) period. It can be seen clearly, that the major part of remaining grid feed-in appears in cooling mode.

The model is capable for analyzing the system design aiming at optimal matching of PV, heating and cooling load and PCM-storage capacity. Figure 4 on the left hand side shows the amount of thermal energy which can be charged (blue) and discharged (red) daily in July for different electrical power ratios of PV and VRF (HP) system.

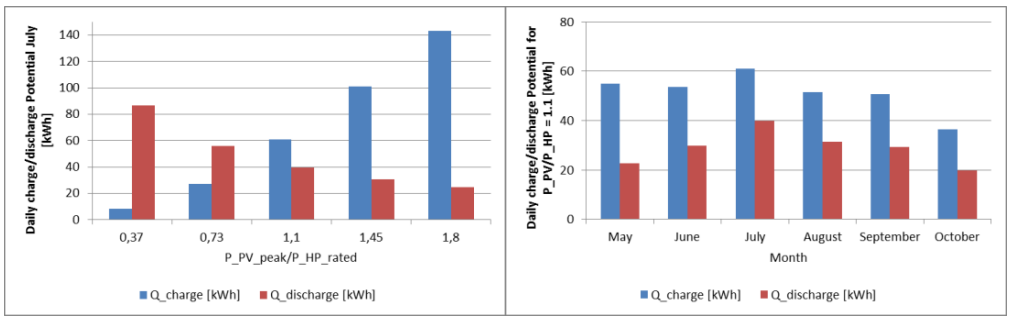

Figure 4 Daily charge/discharge potential of the storage. In July for variable PV-power (left). Daily charge/discharge potential for the entire cooling period with a relation of PV-power/rated power (HP) = 1.1 (right).

While for small scale PV the storage cannot be charged during the day, large scaled PV installations cannot use the stored energy the same day. The diagram on the right hand side shows the results for a slightly oversized PV-plant with a fix power ratio of 1.1. Regarding the average thermal energy which can be charged and discharged in one day during the whole cooling period, a storage capacity between 20 kWh and 30 kWh is found to be suitable for the considered system. It is important to say that this shows the maximum capacity which can be used. Furthermore there can be limits for the useable capacity due to the refrigerant cycle and the implementation/characteristic of the storage. Therefore another model for the cooling circuit and for the PCM-storage had been set up in EES (Engineering Equation Solver). These models are described in the upcoming Chapter.

3. Storage Implementation and Development

3.1. Possible Storage Implementations

As already mentioned there are different options for integration of a PCM-storage into the heat pump cycle. With regard to the desired function different melting temperature ranges can be taken into account. Figure 5 gives a general overview of the different possible storage functions and their operation. The left side shows the functions with the temperature range of each application, while on the right side a description of the cyclic operation of the system is given with charging and discharging phases.

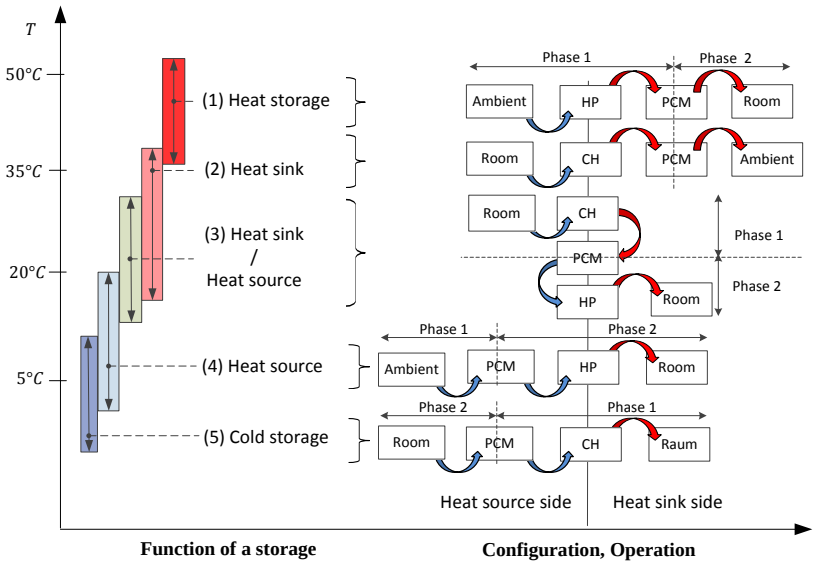

Figure 5 Different implementations of the Storage. Function of the storage with corresponding application temperature (left). Phases of operation on the right for chiller (CH) and heat pump (HP) applications (right). (Loistl et al., 2017)

For example configuration (1) represents a heat storage. In phase one the storage is charged with energy by heat pump (HP) operation, using the ambient as heat source. Subsequently in phase 2 the energy can be used for a heating purpose. Due to results of the TrnSys modelling phase, the possibilities to implement the storage as central cold storage (5), or as subcooler, which can also be categorized as heat sink were considered in more detail. For that purpose an EES model for the cooling circuit had been set up.

The model comprises enthalpy balances for the different steps of the refrigerant cycle characterized by the state points listed in table 2. For the refrigerant the dataset of R410A is used, which is the common refrigerant in state of the art VRF-systems.

Tab. 2: State points of the modelled refrigerant circuit.

Number	Definition
[1]	Beginning of Vaporising
[2]	End of Vaporising
[3]	Superheat of refrigerant
[4]	Hotgas after Compressor
[5]	Hotgas, beginning of Condensation
[6]	Liquid refrigerant, end of condensation
[7]	Liquid, subcooled refrigerant

The considered VRF-system operates with nearly fixed levels of evaporating and condensing temperatures. The following log(p)/h diagrams respect that with the shown isotherms for $T_{Condens}$ and T_{Evap}.

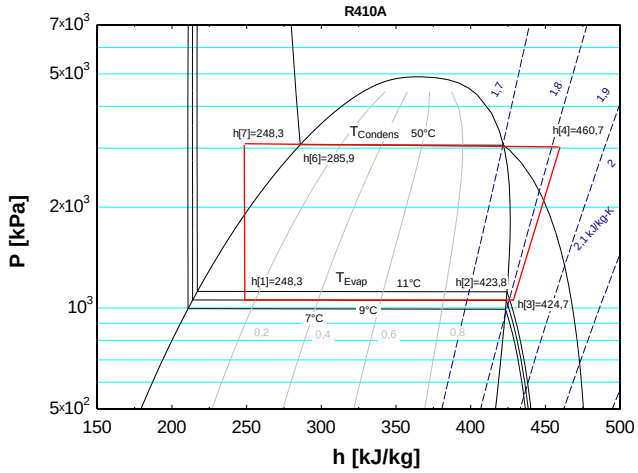

Figure 6 log(p)/h diagram. Example for the calculation of the refrigerant cycle.

Figure 6 shows the cycle state points in a log(p)/h diagram as given in Table 2 for the common system without any modifications of the refrigerant cycle. In this example the system works at its nominal cooling capacity of 22.4 kW with an evaporating temperature of 9 °C and a condensation temperature of 50 °C. The superheating is set to 4 K and the isentropic efficiency of the compressor is assumed to 0.7.

For a better understanding of the system, the storage configuration as subcooler is shown more detailed.

PCM-Storage working as subcooler

One possible implementation of the storage is to use it as additional subcooler in the refrigerant cycle. The idea using a thermal storage for subcooling the refrigerant is not completely new. The Electric Power Research Institute in California already worked on a combination of a VRF-system using an ice-storage for subcooling (Amarnath, 2009). The ice-storage there was charged in nighttime and discharged during the day to prevent peak loads. The main difference to this approach in the present investigation is the possibility to charge the storage in parallel to the regular cooling operation. Therefore it will be possible to charge the storage when PV-peaks occur.

First a simplified P&ID scheme of each storage implementation in case of charge (left hand side) and in case of discharge (right hand side) is shown. The scheme is reduced to a 2-pipe system working in cooling mode. The P&ID is followed up by the corresponding log(p)/h diagram both in case of charge (left) and discharge (right).

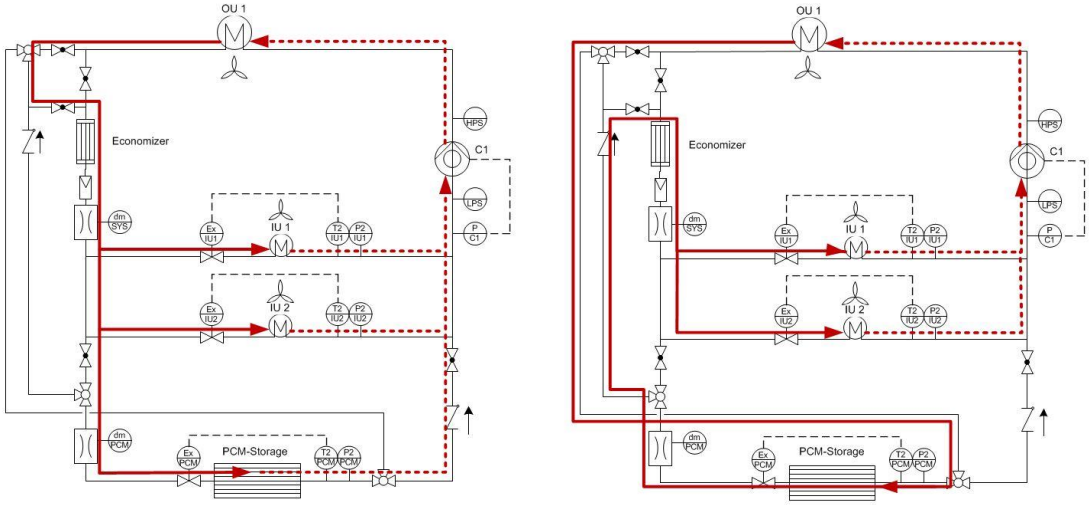

Figure 7 P&ID VRF system with a storage working as subcooler. 1 Outdoor Unit (OU), 2 Indoor Units (IU), Economizer and the PCM-Storage. Charging PCM-Storage on the left. Discharging PCM Storage on the right hand side.

Figure 7 shows on the left hand side the charging of the storage at the common evaporating level of the system, using PV surplus energy. Therefore, the phase change temperature has to be above this level. While charging, the storage is connected to the system like an additional Indoor Unit. Using the common evaporating level, there are no EER losses expected while charging. The storage works as additional load. Due to a higher part load ratio, positive effects on the EER while charging are expected. The right hand side of the P&ID shows the discharge case. When thermal load exceeds solar supply, the liquid refrigerant is led through the storage and is subcooled near the melting temperature of the chosen material. The already subcooled refrigerant is now led through the conventional economizer to ensure safely a sufficient subcooling before the refrigerant is led to the Indoor Units.

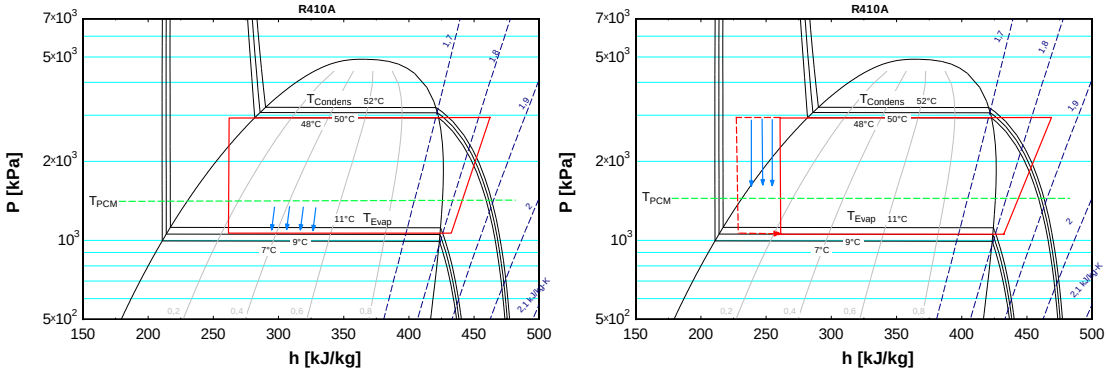

Figure 8 PCM storage used as additional subcooler in case of discharge (right). Charging on the common evaporating level of the system (left).

Figure 8 illustrates the refrigerant cycle of the process while charging (left) and discharging (right). The green line represents the melting temperature of the PCM, which has to be above the common evaporating temperature. With the storage used as subcooler there are two benefits to achieve:

- A higher usable enthalpy difference for cooling compared to conventional subcooling.
- Reaching sufficient subcooling by the storage can relieve the conventional economizer. Those systems usually subcool the refrigerant by evaporating a part of the condensed refrigerant to low pressure level. This part of the refrigerant is lost for the energy conversion but has to be transported by the compressor.

Both benefits lead to an increase of the EER during the discharge phase of the storage compared to conventional systems. This gives the possibility for a lower electrical demand when it is appropriate.

Figure 9 shows the EER improvement of the system at discharging the storage over varying melting temperature for the PCM-storage. It is assumed that the system works on its nominal conditions at an evaporating level of 9 °C. Lower melting temperatures improve the subcooling and also the EER up to 24% during the discharging cycle. On the other hand, a sufficient temperature difference between melting temperature and evaporating temperature needs to be ensured in case of charging. Taking both into account, the ideal melting temperature range for this implementation is between 16 °C and 21 °C. It has to be stated that the increased evaporator efficiency and the related improvement of the EER is a result of an additional input of driving energy during loading of the storage. Integrally, only minor changes of the average EER of the system should occur, related to the change of the load profile along the day.

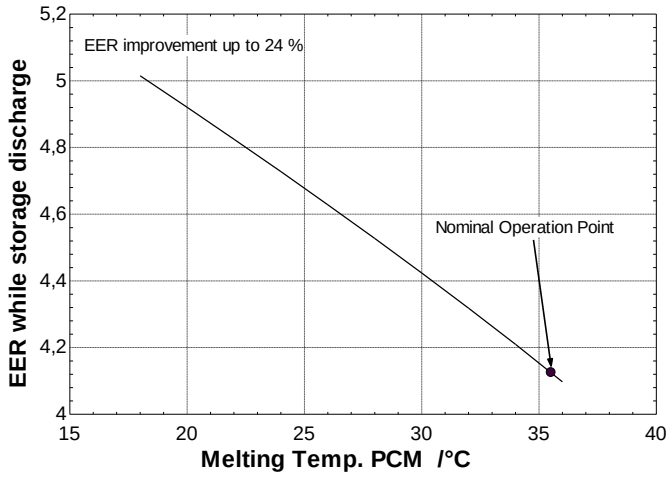

Figure 9 EER improvement in case of discharge for different melting temperatures of the PCM. Comparison to the nominal operation point of the system (storage working as subcooler).

3.2. Sizing/Development of Subcool Storage

Selection of storage material

Since it has been determined that the storage for the pilot installation should be working as a subcooler, a PCM material with a melting range around 16 °C and 21 °C had to be found. Besides a fitting melting point other important factors were a high latent heat and an economically viable price. To improve heat transfer rates it was decided to work with a metal heat exchanger. Hence a non-corrosive storage material was needed which excluded most salt-hydrates.

Regarding the temperature range, paraffin waxes are a good alternative. Their advantages include non-corrosivity, freezing without much supercooling, the ability to melt congruently, no segregation and they are non-hazardous. Parafol 16-97 from Sasol with an onset temperature around 16.5 °C, a latent heat of at least 220 J/g was found to be suitable(Sasol Performance Chemicals, 2017). The relatively low melting temperature range around 18 °C ensures a high temperature difference to the condensation point and therefore leads to a higher EER gain.

Since Parafol 16-97 like most paraffin waxes has a low thermal conductivity, graphite powder will be added to the storage medium to improve the thermal conductivity and allow higher power rates. The used graphite is SIGRATHERM® GFG 600. Tests with the mixture showed that with a mass ratio of 1:5 the thermal conductivity is sufficient and the mixture is still pumpable and therefore easy to fill into the storage container.

Construction of the storage unit

The test building is the institute of the ZAE Bayern located in Garching, Bavaria. Figure 10 shows the modeling result for the available cooling output of the PV driven VRF system and the cooling demand for a typical cooling day in August (left) and a day in transition time at the beginning of May (right, day with solar radiation). The data was generated by available weather data and the TrnSys model explained in chapter 2. Electricity is generated by photovoltaic panels. This electrical power is used to run the cooling cycle of the VRF system. The calculated possible total thermal power output is shown in red. The cooling demand of the building is shown in blue. The difference between available cooling power and cooling demand is shown in green (excess thermal energy) and black (cooling demand exceeding the thermal power output). Due to the lightweight construction of the investigated building, the cooling demand and the solar peak correlate very well as shown in Figure 10. Hence the potential for a load shift is comparably small. The analysis of the data from April to October, which are the months with a sizeable cooling demand in Germany, suggested a storage capacity of about 20 kWh to be sufficient. Would a building with a heavier construction with building materials such as concrete or stone be used, it would take a longer time to heat up the interior. The cooling demand would shift to a later time and therefore the peaks of demand and production would not correlate so well. This would lead to a bigger storage demand.

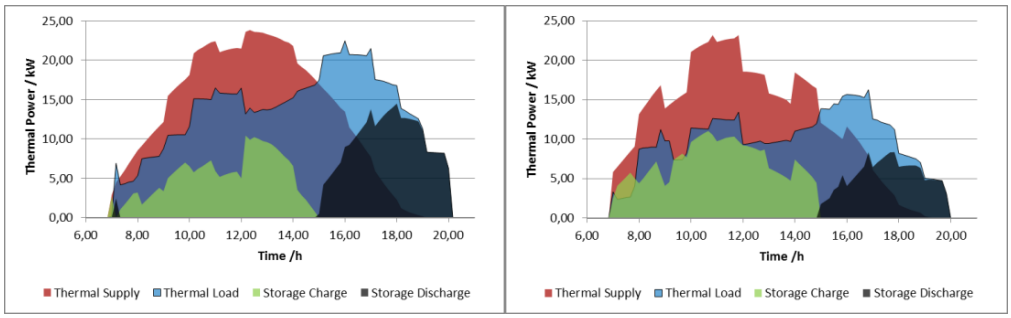

Figure 10 Exemplary thermal course of a typical cooling day for August (left). Thermal course of a day in transition time with solar radiation in May (right). The storage charge (green) and discharge (black) areas are representing potentials.

However, the possible maximum charging and discharging power is not arbitrary, but is limited by the construction of the storage and the heat exchanger. Furthermore it is influenced by the charging history. Hence, an iterative process was necessary to determine an appropriate storage size and heat exchanger construction.

First the volume of the storage container was calculated with the estimated 20 kWh storage capacity. A suitable heat exchanger was modelled using the Engineering Equation Solver (EES) software. Afterwards, the charging and the discharging process were simulated.

Charge

The cooling fluid R410A is injected into the heat exchanger of the storage unit and evaporates, cooling the PCM material. As a result, the selected PCM Parafol 16-97 crystallizes along the heat exchanger. The model took into account the evaporation of cooling fluid on the inside of the heat exchanger as well as the heat transfer through and the phase change in the PCM material. It includes different pressure loss phenomena (static, acceleration, frictional, pipe bends) and the flow boiling effects after Shah (VDI-Gesellschaft Verfahrenstechnik und Chemieingenieurwesen, 2002, Nellis and Klein , 2009). Depending on the distance between phase front within the Parafol 16-97 and the heat exchanger the transferable power varies.

Therefore, the maximum transferable power depends on the way the storage was charged and discharged before. To simplify the model it was assumed that each day was independent of the one before. That means the storage was discharged every morning. The system is not highly reactive, meaning switches between charging and discharging in a short time scale are not favorable. Therefore one can assume that there is only one charging and one discharging cycle per day. Under these assumptions, the possible power transfer is a function of the state of charge (SoC) of the storage, because the distance between the heat exchanger surface and the phase front in the PCM is growing with a larger SoC. The higher the SoC, the larger is the fraction of PCM in the solid state.

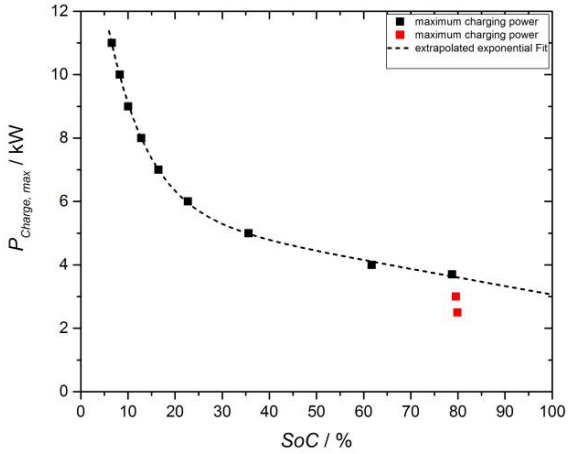

Figure 11 Maximum charging power depending on the SoC

Figure 11 shows the maximum transferable charging power depending on the SoC. Until about 80% of SoC it can be fitted by an exponential function. At higher SoC values (red squares) the maximum charging power decreases rapidly. This is because in the simulation the phase fronts reach symmetric borders at that point. Consequently, the calculated heat exchange surface decreases rapidly, which reduces the transferable power. However, in this simplified model heat transfer parallel to the heat exchanger was not considered. Therefore it is expected, that the decline in the maximum transferable power is not that sharp in a real storage device. This was already confirmed in preliminary tests. For further calculations, the exponential fit was extrapolated to a SoC of 100%.

To calculate the maximum charging energy, the minima of the available thermal power and the maximum possible charging power resulting from the actual SoC were determined.

Discharge

During discharging liquid R410A is injected at high pressure and temperature into the heat exchanger of the storage unit. Within the storage, the cooling fluid is cooled from about 48 °C to nearly the phase change temperature of the PCM (18 °C), melting Parafol 16-97. The maximal possible discharge power can be calculated via equation 1.

$$P_{Discharge} = \dot{m}_{R410A} \cdot \int_{T_c}^{T_h} c_{p,l}(T) \cdot dT \qquad \text{(eq. 1)}$$

Hereby $P_{Discharge}$ is the maximum discharge power. $\dot{m}_{R410A}$ is the mass flow rate of the cooling liquid, $c_{p,l}(T)$ the temperature dependent heat capacity, and T_h and T_c are the temperatures at the in- and outlet of the PCM storage unit. The mass flow rate is given by the actual cooling demand. The cooling power is provided by the evaporation of R410A. Hence, the mass flow rate is given by:

$$\dot{m}_{R410A} \approx \frac{P_{Cooling}}{\Delta h_{R410A}} \qquad \text{(eq. 2)}$$

For a fixed inlet temperature T_h of 48 °C the discharge power is found to be limited to about 28% of the cooling power. The excess energy is necessarily provided by the cooling cycle (liquefaction).

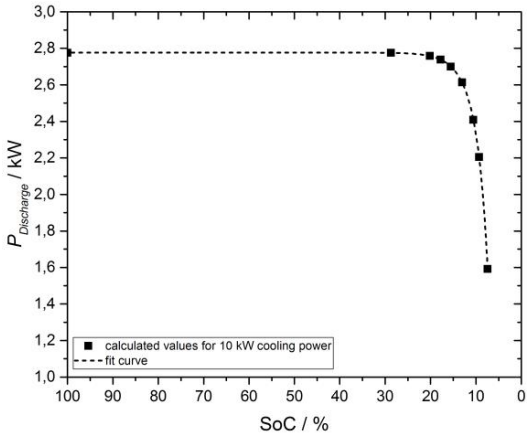

Figure 12 Discharge power depending on the SoC for a cooling power of 10 kW

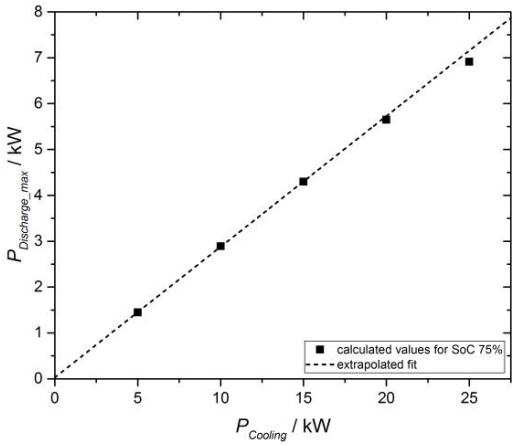

Figure 13 Maximum discharge power depending on the cooling power for a SoC of 75 %

The discharge power is in most cases rather limited by this fact then by the discharge characteristics of the storage unit. Figure 12 shows the SoC dependent discharge power for a cooling power of 10 kW. Down to around 20% SoC the discharge power is virtually constant (100% means the PCM is solid, while 0% means it is liquid). After that there is a fast decay. It results from the heat transfer which in this region limits the discharge power. However, this is a worst case estimation. For example heat conduction parallel to the heat exchanger was not taken into account in these calculations. Hence, it can be expected that the decay is not as steep in reality. In most operating conditions the discharge power will be limited by the cooling power.

In Figure 13 the maximum discharge power is shown as a function of the cooling power for a SoC of 75%. The data yields a nearly linear relation. Only at very high power rates the slope flattens. It confirms that the discharge power is generally limited by about 28% of the cooling power.

Hence, the calculation of the maximum theoretical available discharge energy per day was simplified and calculated by multiplying the cooling demand with a factor of 0.28 when cooling demand exceeds the generated cooling output of the VRF system.

Results of the iteration

The found limits of charging and discharging power have been implemented in the system model. For each day of the cooling period a possible maximum thermal energy which can be shifted was calculated again. These restrictions on the transferable power led to a lower reasonable storage size. The iterative process was continued and a latent heat storage capacity of 16 kWh was determined.

The final heat exchanger unit contains six heat exchangers with each 23 m length which will enable the storage to a peak power of more than 10 kW while charging.

The storage dimensions will be 1400 x 600 x 600 mm. 390 l of the PCM-Graphite compound will be used. This corresponds with a latent heat capacity of 16 kWh. A schematic drawing of the storage and the heat exchanger unit is shown in Figure 14.

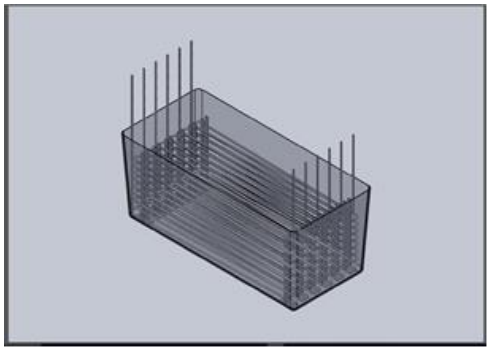

Figure 14 Schematic drawing of the storage container and the heat exchanger

3.3. Implementation of Storage Characteristic to Refrigerant Cycle Model

After the design phase for the storage and the iteration to work out a suitable storage capacity, the characteristic curves for the storage were implemented to the refrigerant cycle model. Figure 15 shows the course of a typical cooling day in August. The data is related to the thermal course shown in Figure 10 on the left representing the theoretical charge and discharge potential independent from the kind of storage implementation.

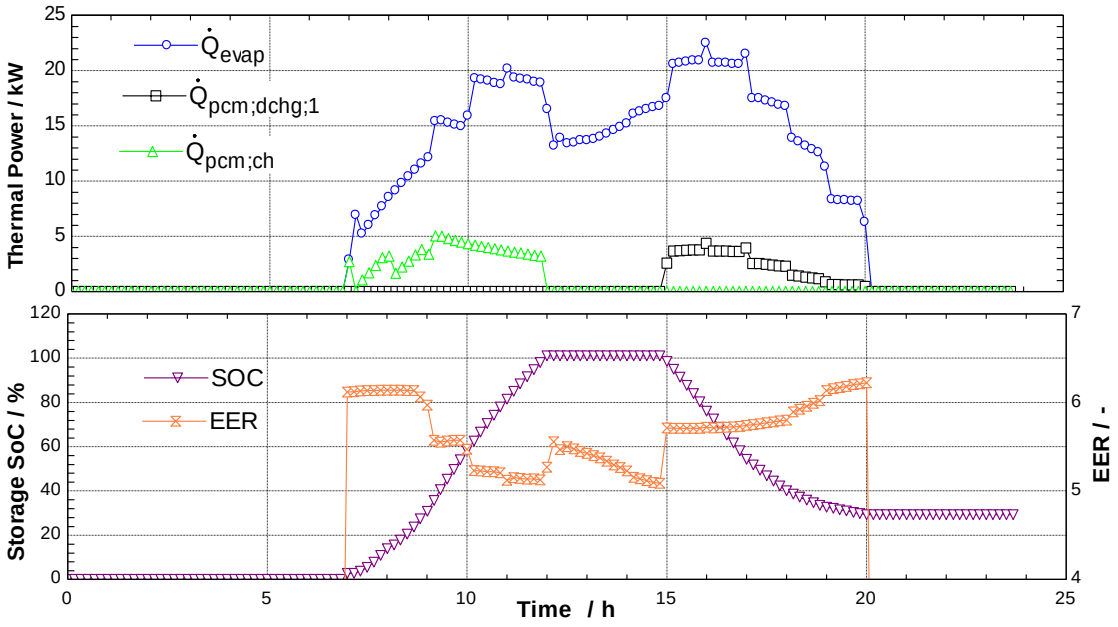

Figure 15 EES model of the refrigerant cycle fed with thermal load data and storage characteristics. Thermal course for a typical cooling day in August (Data out of Figure 10 on the left showing the potential). Thermal load, storage charging and discharging power in the upper part. SOC and EER in the lower part.

The upper part of Figure 15 shows the cooling load (blue, circled) of the system including storage charging. The green line (triangular) represents the storage charging power taking into account the characteristics described by Figure 11. The black line (squares) shows the possible discharge of the storage with respect to the limitation through the current thermal load. The bottom part of Figure 15 shows the variation of the systems EER (orange curve) and the storage SOC (violet, triangular) during the day. As already mentioned due to a higher part load ratio while charging, a slight EER-gain through charging can be expected. The real benefit is shown when discharge begins at 15:00 pm and the EER increases from 5 to nearly 6.

This EER gain while discharging the PCM-storage will significantly reduce electrical load when it is appropriate. In this example, the storage will be completely charged before the PV peak occurs. Thus, the course of the SoC trend line directly indicates that measures have to be taken for controlling the operation of the storage. A predictive control strategy is required in order to charge the storage completely while covering the PV-peak.

4. Summary and Outlook

The study describes the modelling and sizing phase for a PV driven VRF system coupled with a thermal PCM-storage. The integration of the storage as subcooler is described in detail. Considering the thermal load, PV-supply and the systems boundary conditions an adequate PCM was chosen and a storage with sufficient thermal characteristic was designed.

Next steps are the installation and start-up of the VRF pilot installation in Garching. In parallel the designed PCM-storage will be built up for laboratory tests. In a second step a tested and optimized pilot-storage will be implemented to the VRF installation. For the integration of the PV peak without losses of solar fraction, predictive control strategies will be worked out and tested during operation of the system.

5. References

Amarnath K., 2009. Performance Assessment of a Variable Refrigerant Flow Air Conditioner with Ice Storage System. Electrical Power Research Institute, Palo Alto, California

Fujitsu General Limited, 2014, Design and Technical Manual Airstage VR-II Variable Refrigerant Flow System, Japan

Loistl, F., Korth, T., Schweigler, C., 2016. Einsatz von Latentwärmespeichern in Klimageräten, Deutsche Kälte- und Klimatagung, Kassel

Loistl, F., Korth, T., Schweigler, C., 2017. Latentwärmespeicher für Luft/Luft-Wärmepumpen, KI – Kälte-, Luft- und Klimatechnik, p. 50-55, 10/2017

Nellis, G., Klein, S., 2009. Heat Transfer, Cambridge University Press, New York

Sasol Performance Chemicals, PARAFOL C12–C22, High purity normal paraffins, http://www.pcm-ral.org/pcm/wp-content/uploads/2016/08/Brochure_PARAFOL_2016.pdf, [Stand 05.10.2017]

VDI-Gesellschaft Verfahrenstechnik und Chemieingenieurwesen, 2002. VDI-Wärmeatlas: Berechnungsblätter für den Wärmeübergang, Heidelberg

Weniger, J., Bergner, J. Tjaden, T., Quaschning, V., 2015. Dezentrale Solarstromspeicher für die Energiewende. Hochschule für Technik und Wirtschaft Berlin

Acknowledgment

The project SolarSplit is funded by the BMWi (German Federal Ministry for Economic Affairs and Energy) under grant No. 0325900A, B and C.